Modelling of solid / liquid fractionation of trace metals for suspended sediments according to the hydro-sedimentary conditions of rivers - Application to 137Cs in the Rhône River (France)

Wirginia Tomczak, Patrick Boyer, Frederique Eyrolle, Olivier Radakovitch, Mohamed Krimissa, Hugo Lepage, Muriel Amielh, Fabien Anselmet

Modelling of solid / liquid fractionation of trace metals for suspended sediments according to the hydro-sedimentary conditions of rivers
- Application to ^{137}Cs in the Rhône River (France) -

Wirginia Tomczak[1], Patrick Boyer[1], Frederique Eyrolle[1], Olivier Radakovitch[1], Mohamed Krimissa[2], Hugo Lepage[1], Muriel Amielh[3], Fabien Anselmet[3]

1 - Institut de Radioprotection et de Sûreté Nucléaire (IRSN), PSE-SRTE-LRTA, Cadarache, France

2 - Electricité de France (EDF), Recherches & Développements, Chatou, France.

3 - Aix Marseille Université, CNRS, Centrale Marseille, IRPHE U.M.R.7342, Marseille, France.

*Corresponding author:

E-mail address: patrick.boyer@irsn.fr (Patrick Boyer)

Highlights:

- Modelling of K_d according to hydro-sedimentary conditions
- Particle size effect on K_d
- Geochemical background effect on K_d
- Colloidal pumping effect on K_d.

Abstract

The behavior and impact of trace metals discharged into rivers depend on their solid/liquid fractionation and the fate of these two phases according to hydro-sedimentary processes. The solid/liquid fractionation depends on many environmental factors which imply uncertainties of several orders of magnitude in the evaluation of the partition coefficients, whether by geochemical modelling, in situ measurements or sorption-desorption experiments. In this context, this paper presents a model of solid/liquid fractionation of trace metals with suspended sediments in rivers which integrates the hydro-sedimentary conditions and the properties of the watershed. Its comparison with the ^{137}Cs concentrations measured in the Rhône River (France) shows that the solid/liquid fractionation of ^{137}Cs with suspended sediments in rivers depends on chemical processes but also and above all on variations in water flow rate, size and load of suspended sediments and the balance between anthropogenic discharges and the average trace metal content of soils in the watershed.

Keywords: K_d modelling; river systems; suspended sediments; particle size; trace metal; colloidal pumping.
Published as : Tomczak et al., Environmental Modelling and Software, 2021
doi : 10.1016/j.envsoft.2021.105211

1 Introduction

Within the framework of environmental and human health risk assessment; transport and bioavailability of trace metals (TMs) in aquatic environments were thoroughly investigated. Most TMs from anthropogenic origins such as industrial/urban wastewaters or agricultural uses are delivered to aquatic systems as inorganic complexes or hydrated ions, which are more or less adsorbed onto sediment particles (Vuković *et al.*, 2011). Consequently, their behavior in aquatic systems strongly depends on their solid/liquid fractionation which governs their mobility, bioavailability, transport and residence time.

In rivers, suspended sediments (SS) play a major role on such distribution because they constitute important TMs carriers due to their high capacity of adsorption (Xia et al., 2004). SS behavior and fate are governed by various hydro-sedimentary processes including particle transport/dispersion, sedimentation, early diagenesis and erosion (Walling and Moorehead, 1989).

Among the various SS properties, the particle size is widely known as an important parameter involved in the sorption of TMs because it directly defines the solid surface exchange availability. Most generally, exchange surface availability increases with the decreasing size of particles and the coarser particles adsorb less TMs than the smaller ones (Town and Filella, 2002; Payne et al., 2011). This has been thoroughly demonstrated for various TMs such as Cd (Fan et al., 2017), Hg (Boszke et al., 2004), ^{110m}Ag, ^{58,60}Co and ^{54}Mn (Ciffroy *et al.*, 1995) and ^{137}Cs and ^{210}Pb (He and Walling, 1996).

Furthermore, it is well established that the transport modes of SS (Crosby and Whipple, 2004) and the processes of sedimentation (Gibbs *et al.*, 1971; Abarca *et al.*, 2017) and erosion (Xia *et al.*, 2004) are particle size dependent. Particles smaller than 200 µm are generally suspended and easily transferred by water flows unlike coarser particles (Palmateer *et al.*, 1993; Fan *et al.*, 2017).

Due to these mechanisms, the particle size of SS explains most of TMs contents and fluxes within the water column (Sigg *et al.*, 2000; Turner *et al.*, 2002; Reynolds *et al.*, 2010; Boyer *et*

al., 2018). It is therefore a fundamental parameter for the modelling of the solid/liquid partitioning of TMs in rivers. In addition, this fractionation is also time dependent so that equilibrium is not instantaneous but reached after several hours or days depending on the metal and the environmental conditions. Although kinetic models exist (Cameron and Klute, 1977; Garcia-Sanchez *et al.*, 2014), their parameters are poorly documented and the K_d approach remains the most common operational means to assess solid / liquid fractionation of TMs assuming instantaneous equilibrium and reversibility:

$$K_d = \frac{C_s}{C_l} \quad [m^3.kg^{-1}] \qquad \text{(Eq. 1)}$$

Where C_s [$xx \cdot kg_{dry}^{-1}$] and C_l [$xx \cdot m^{-3}$] are the TMs contents of the solid and liquid phases, with xx = kg, mol or Bq.

Due to the kinetic effects, a K_d is nothing more than the ratio of the sorption and desorption kinetics and it must be kept in mind that the equilibrium assumption limits its application domain to contact times sufficiently long to reach these conditions. Because sorption kinetics are generally faster than desorption kinetics (Pèrez *et al.*, 2015), two types of K_d have been introduced for operational applications (Ciffroy *et al.*, 2009; Boyer *et al.*, 2018): a K_d sorption to represent the rapid equilibrium reached when sorption processes are dominant, as in a sorption experiments and downstream of a point of discharge, and a K_d desorption to represent situations dominated by desorption processes such as in a desorption experiments and the long-term behaviour of watersheds and bottom sediments contamination. Anyway, the K_d approach remains a black box that aggregates physicochemical processes such as hydrogen bonding, electrostatic and van der Waals forces, surface precipitation and surface co-precipitation (Heling *et al.*, 1999; Durrieu *et al.*, 2006), as well as biochemical processes such as microbial alkylation and volatilization that can change, independently of solid-liquid exchanges, the solution concentrations of elements such as selenium, arsenic and mercury (Peitzsch *et al.*, 2010). At the same time, these processes are dependent on the chemical speciation of TMs and numerous environmental factors: pH (Lu and Allen, 2001; Wang *et al.*, 2017), nature and load of SS (Apte *et al.*, 1995; Dominik *et al.*, 2007; Jweda *et al.*, 2008; Boyer *et al.*, 2018), dissolved organic carbon content (Barreto *et al.*, 2011; Zhang *et al.*, 2013), temperature (Warren and Zimmerman, 1994), ionic strength (Duc *et al.*, 2013). As a consequence of this complexity, the K_d values vary over several orders of magnitude even for a single TM and a single river as has

been shown by different K_d values compilations (Allison and Allison, 2005; Durrieu *et al.*, 2006; Ciffroy *et al.*, 2009; Boyer *et al.*, 2018; Tomczak *et al.*, 2019).

In practice, K_d values are determined by in situ measurements, sorption-desorption experiments in laboratories and different modelling approaches such as parametric models (Sheppard *et al.*, 2009; Sheppard, 2011), dynamic models (Garcia-Sanchez *et al.*, 2014) and mass-action based on thermodynamic models (Tipping, 1994; Goldberg *et al.*, 2007).

However, these different approaches are mainly based on geochemical concepts and remain difficult to apply at the temporal and spatial scales of a river for those they require to be coupled to hydro-sedimentary models (Garneau *et al.*, 2017) and to measure or assess a number of environmental variables (Ilina *et al.*, 2020). Moreover, and despite the central role of particle sizes in the solid/liquid fractionation of TMs with SS, this parameter is poorly considered by these models while, at the same time, it is little documented by the scientific literature related to K_d values for river systems. Thus, the effect of particle size in the models of transfer of TMs in rivers is generally overlooked and, to our knowledge, the only K_d models including specifically the particle sizes are those proposed by He and Walling (1996) and Abril and Fraga (1996).

He and Walling (1996) performed sorption experiments on various size fractionated samples of soils and sediments and showed that K_d values for ^{137}Cs and ^{210}Pb are closely correlated to the specific surface area, SSA [$m^2 \cdot kg^{-1}$], through an empirical power function:

$$K_d = a \cdot SSA^b \qquad \text{(Eq. 2)}$$

Abril and Fraga (1996) and Abril (1998a) proposed a more mechanistic approach that reproduces this empirical relation by considering spherical particles and assuming that only a fine external layer of thickness δ participates to the ionic exchanges within the surrounding water medium, instead of the whole solid particle. Compared to the approach of He and Walling (1996), based only on the raw SSA, the thickness δ can be considered as a correction factor which completes the exchange surface with the porous surface layer of the particles at the inside in which TMs can diffuse according to their properties. Thus, they considered that only the TMs associated with this reactive external layer are exchangeable with the solution while those in the non-reactive internal part are not exchangeable (Figure 1).

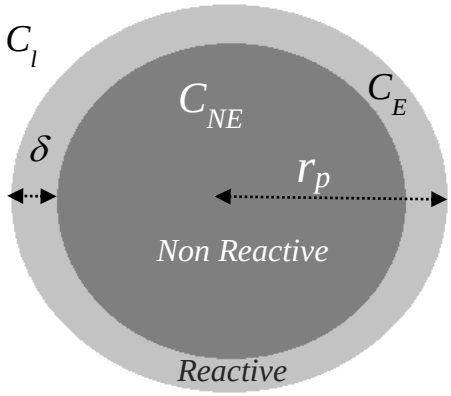

Figure 1: Abril and Fraga (1996) theoretical modelling concepts for spherical particles.

C_l: liquid concentration; C_{NE}: non-exchangeable concentration; C_E: exchangeable concentration; r_p: radius; δ: thickness of the exchange layer

Additionally, they assumed equilibrium between the TMs contents in the reactive layer and in the solution such as:

$$K_{d\delta} = \frac{C_E}{C_l} \quad \text{(Eq. 3)}$$

Where $K_{d\delta}$ is the K_d for the TMs in the reactive layer of thickness δ [µm] and C_l [xx.l^{-1}] and C_E [xx.kg_{dry}^{-1}] are the concentrations in the liquid phase and in the exchangeable part of particles, respectively.

Based on these theoretical concepts, the K_d of a particle can be expressed as a function of its radius r_p [µm]:

- if $r_p > \delta \Rightarrow K_d = K_{d\delta} \cdot \left(1 - \left(1 - \frac{\delta}{r_p}\right)^3\right) + K_{d\delta} \cdot \frac{C_{NE}}{C_E} \cdot \left(1 - \frac{\delta}{r_p}\right)^3$ (Eq. 4)
- if $r_p \leq \delta \Rightarrow K_d = K_{d\delta}$ (Eq. 5)

In these relationships, r_p is specific to particles, δ and $K_{d\delta}$ are specific to geochemical conditions and C_{NE} [xx· kg_{dry}^{-1}] is specific to the environmental context.

Figure 2 presents the evolution of $K_d/K_{d\delta}$ as a function of C_{NE}/C_E and δ/r_p according to this model.

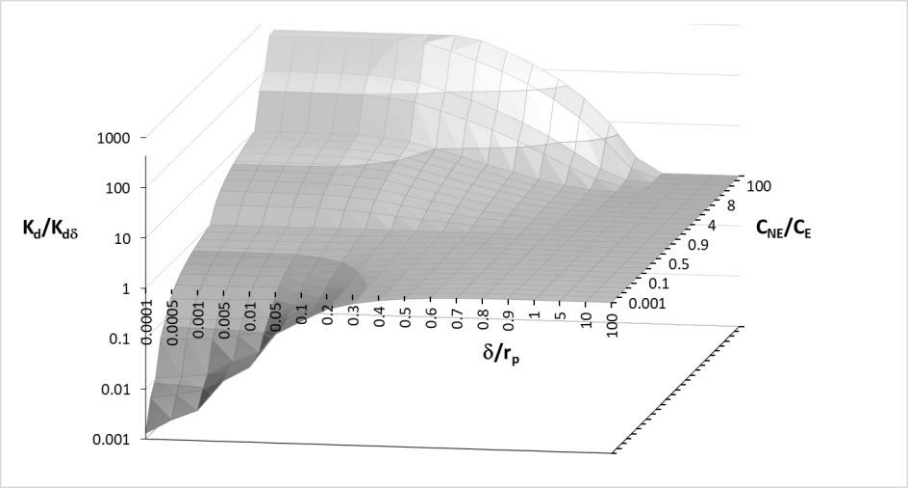

Figure 2: $K_d/K_{d\delta}$ ratios as a function of C_{NE}/C_E and δ/r_p ratios according to the Abril and Fraga Model

According to the Abril and Fraga Model (labelled AFM), K_d is equal to $K_{d\delta}$ when particle sizes are smaller than the reactive layer thickness δ and when the ratio C_{NE}/C_E is close to one (Figure 2). For particle sizes greater than δ, K_d decreases with r_p rising and C_{NE}/C_E decreasing, which corresponds to situations where the concentrations of anthropogenic TMs onto the surface of particles are clearly above those within the mineral. In contrast, K_d increases when r_p is high and C_{NE}/C_E is high, corresponding to situations dominated by the geochemical background of TMs.

This modelling approach highlights that changes in C_E, C_{NE} and r_p are sufficient to induce a variation of the K_d over several orders of magnitude, as is the case in most rivers (Tomczak *et al.*, 2019). In this context, we propose an adaptation of the AFM in order to determine the K_d of the TMs for SS in rivers according to the particle sizes, the hydro-sedimentary properties of the river and the geochemical context of the watershed. This adaptation was tested on a ^{137}Cs dataset acquired in the Rhône River (France) from long term monitoring. The results highlight its relevance to explain the variations of the K_d values which were observed over several years according to the water flow rate.

2 Method

For situations dominated by anthropogenic TMs ($C_{NE}/C_E < 1$), several field studies (Honeyman and Santschi, 1988; Benoit and Rozan, 1999; Eyrolle *et al.*, 2006) and data compilations (Boyer *et al.*, 2018; Tomczak *et al.*, 2019) show that K_d tends to decrease when the load of suspended sediments, labelled [SS], increases. This trend is explained by three major mechanisms which are: 1) particle size effect, 2) mass/volume ratio effect and 3) colloidal pumping.

1) The effect of particle size reflects that [SS] and the mean radius of suspended particles both tend to increase with increasing water flow rate. Observed in most cases (Müller and Förstener, 1968; Metha, 2014) but not all (Walling *et al.*, 2000), this tendency leads to a decrease in the mean specific surface area of SS when [SS] increases and therefore to lower K_d values.

2) The mass/volume effect (Abril, 1998b) concerns particle sizes larger than δ and depends on the balance between the total concentrations added to the rivers by the anthropogenic discharges (C_D [xx.m^{-3}]) and the background of the TMs contents in the watershed (C_{soil} [xx.kg^{-1}]) which can be assimilated to C_{NE}. This background is related to the presence of natural TMs and/or non-reversible solid fractions of anthropogenic TMs due to industrial and agricultural uses or past atmospheric fallouts and which have "migrated" within the non-reactive crystalline structure of the minerals. In the case where C_D is negligible, an increase of [SS] changes the solid concentrations little at the same time that it increases the liquid concentrations, resulting in a decrease of K_d. The AFM indicates that this trend is reversed when C_D is sufficiently strong compared to C_{soil} with a theoretical limit given by $C_D > C_{soil}/K_{d\delta}$.

3) Finally, colloidal pumping also explains the decrease of K_d together with the rise in [SS] because the concentration of colloidal compounds increases mechanically at the same time as [SS] when the water flow rate increases. These sub-micro particles are poorly retained by filtration and it has been widely demonstrated that they are the most efficient particles to adsorb TMs (Li et al., 1984). Consequently, an increase in their concentrations enriches the TMs contents of the filtered water (Honeyman and Santschi, 1988; Benoit and Rozan, 1999) and reduces the K_d values.

The AFM integrates the effects of points 1 and 2 by the first and second terms in equation 4, respectively. In order to integrate the colloidal pumping effect, let us consider that the liquid phase is composed of the dissolved and colloidal fractions:

$$C_l = C_d + C_c \cdot [SC] \quad \text{(Eq. 6)}$$

Where C_c [xx·kg^{-1}] is the TM concentration within the colloidal phase, [SC] [kg·m^{-3}] is the concentration of colloids, C_d [xx·m^{-3}] is the dissolved TM concentration and C_l [xx·m^{-3}] is the TM concentration in the total liquid phase.

In this case, $K_{d\delta}$ is replaced by $K_{d\delta}{}^*$ which is given by:

$$K_{d\delta}{}^* = \frac{C_{SS,E}}{C_l} = \frac{C_{SS,E}}{C_d \cdot (1 + K_{dc} \cdot [SC])} = \frac{K_{d\delta}}{1 + K_{dc} \cdot [SC]} \quad \text{(Eq. 7)}$$

Where $C_{SS,E}$ [xx.kg^{-1}] is the exchangeable concentration of TMs inside the reactive fraction of SS and K_{dc} [l.kg^{-1}] is the K_d of colloids.

The δ values obtained by Abril et Fraga (1996) for Pu, Cs and Zn are 0.78, 1.96 and 5.17 µm respectively. These values are all greater than the size of colloidal particles (< 0.45 µm) which allows us, according to the AFM theory, to assume $K_{dc} \approx K_{d\delta}$.

With these considerations, the adaptation of the AFM to SS in rivers leads to:

- if $r_p > \delta \Rightarrow K_d = \frac{K_{d\delta}}{1 + K_{dc} \cdot [SC]} \cdot \left(1 - \left(1 - \frac{C_{SS,NE}}{C_{SS,E}}\right) \cdot \left(1 - \frac{\delta}{r_p}\right)^3\right)$ (Eq. 8)
- if $r_p \leq \delta \Rightarrow K_d = \frac{K_{d\delta}}{1 + K_{dc} \cdot [SC]}$ (Eq. 9)

Where:

- $C_{SS,NE}$ [xx.kg^{-1}] is the non-exchangeable concentration of TMs inside the non-reactive fraction of SS. It is a specific property of the catchment which depends on the geochemical background for naturally occurring TMs and/or on the anthropogenic background produced by non-reversible fractions generated in the long term by industrial and agricultural uses and atmospheric fallouts. Thus, this concentration can be assimilated to C_{soil} [xx.kg^{-1}], the mean TMs concentrations in the soils of the catchment : $C_{SS,NE} = C_{soil}$

- $C_{SS,E}$ [xx.kg^{-1}], the exchangeable concentration of TMs inside the reactive fraction of SS, depends on the solid/liquid fractionation of C_E [xx.l^{-1}] which is the total exchangeable concentration of TMs in the water volume. This concentration is constituted of C_{EB} [xx.l^{-1}], the total exchangeable concentrations originated from the background concentration of TMs

in the watershed and C_D [xx.l^{-1}], the total concentration of TMs added by industrial liquid discharges:

$$C_E = C_{EB} + C_D \quad \text{(Eq. 10)}$$

The total exchangeable concentrations originated from the background concentration of TMs in the watershed is:

$$C_{EB} = C_{soil} \cdot [SS]_R \quad \text{(Eq. 11)}$$

Where $[SS]_R$ [kg·m^{-3}] is the suspended load of reactive SS given by:

- If $(r_p > \delta) \Rightarrow [SS]_R = [SS] \cdot \left(1 - \left(1 - \frac{\delta}{r_p}\right)^3\right)$ (Eq. 12)
- If $(r_p \leq \delta) \Rightarrow [SS]_R = [SS]$ (Eq. 13)

In complement, we deduce the concentration of non-reactive SS by:

$$[SS]_{NR} = [SS] - [SS]_R \quad \text{(Eq. 14)}$$

The total concentration of TMs added by industrial liquid discharges can be easily assessed in case of complete mixing conditions:

$$C_D = \frac{q_D}{Q_{river}} \quad \text{(Eq. 15)}$$

Where q_D [xx·s^{-1}] is the flux of the anthropogenic discharges within the river and Q_{river}[m^3·s^{-1}] is the river water flow rate.

With this relationship, the model should be applied in a zone of complete mixing and by assuming that the TMs fractions removed from the water column by solid phase sedimentation are negligible, which is generally the case in rivers where the MTs are mainly fixed on the finest particles which have the lowest sedimentation rates.

Finally, the total (T), dissolved (d), colloidal (c), liquid (l) and particulate (SS) concentrations of TMs are given by:

$$C_T = C_d + C_c \cdot [SC] + C_{SS,E} \cdot [SS]_R + C_{Soil} \cdot [SS]_{NR} \quad \text{(Eq. 16)}$$

$$C_d = \frac{C_T - C_{Soil}\cdot[SS]_{NR}}{1+K_{dc}\cdot[SC]+K_{d\delta}\cdot[SS]_R} = \frac{C_E}{1+K_{dc}\cdot[SC]+K_{d\delta}\cdot[SS]_R} \quad \text{(Eq. 17)}$$

$$C_c = K_{dc}\cdot C_d\cdot[SC] \quad \text{(Eq. 18)}$$

$$C_l = C_d + C_c \quad \text{(Eq. 19)}$$

$$C_{SS,E} = K_{d\delta}\cdot C_d \quad \text{(Eq. 20)}$$

$$C_{SS} = \frac{C_{SS,E}\cdot[SS]_R + C_{Soil}\cdot[SS]_{NR}}{[SS]} \quad \text{(Eq. 21)}$$

Furthermore, these concentrations can be decomposed according to the contributions of the anthropogenic discharges (D) and the catchment background (B) with $f_D = \frac{C_D}{C_E}$:

- $C_{d,D} = f_D\cdot C_d$ and $C_{d,B} = (1-f_D)\cdot C_d$ (Eq. 22)
- $C_{c,D} = f_D\cdot C_c$ and $C_{c,B} = (1-f_D)\cdot C_c$ (Eq. 23)
- $C_{l,D} = f_D\cdot C_l$ and $C_{l,B} = (1-f_D)\cdot C_l$ (Eq. 24)
- $C_{SS,D} = \frac{K_{d\delta}\cdot C_{d,D}\cdot[SS]_R}{[SS]}$ and $C_{SS,B} = \frac{K_{d\delta}\cdot C_{d,B}\cdot[SS]_R + C_{Soil}\cdot[SS]_{NR}}{[SS]}$ (Eq. 25)

We can then define the K_d specifically to the anthropogenic discharges and to the catchment background by:

$$K_{d,D} = \frac{C_{SS,D}}{C_{l,D}} \text{ and } K_{d,B} = \frac{C_{SS,B}}{C_{l,B}} \quad \text{(Eq. 26)}$$

These different calculation steps are summarized in Table 1.

Table 1: Summary description of the model

(See text for the description of parameters)

Input parameters	
δ, $K_{d\delta}$, K_{dc} ($\sim K_{d\delta}$), Q_{river}, [SS], [SC], r_p, C_{soil}, q_D (or $C_D = \frac{q_D}{Q_{river}}$)	
1 - Calculation of the reactive and non-reactive loads of SS	
• If $(r_{50} > \delta) \Rightarrow [SS]_R = [SS]\cdot\left(1-\left(1-\frac{\delta}{r_p}\right)^3\right)$ • If $(r_{50} \leq \delta) \Rightarrow [SS]_R = [SS]$ • $[SS]_{NR} = [SS] - [SS]_R$	
2 - Calculation of the total exchangeable and non exchangeable TMs concentrations	
• $C_{EB} = C_{soil}\cdot[SS]_R$	• $C_E = C_D + C_{EB}$

• $C_D = \frac{q_D}{Q_{river}}$	• $f_D = \frac{C_D}{C_E}$
4 - Calculation of the dissolved, colloidal and liquid TMs concentrations	
• $C_d = \frac{C_E}{1+K_{dc}\cdot[SC]+K_{d\delta}\cdot[SS]_R}$ • $C_c = K_{dc} \cdot [SC] \cdot C_d$ • $C_l = C_d + C_c$	• $C_{d,D} = f_D \cdot C_d$; $C_{d,B} = C_d - C_{d,D}$ • $C_{c,D} = f_D \cdot C_c$; $C_{c,B} = C_c - C_{c,D}$ • $C_{l,D} = f_D \cdot C_l$; $C_{l,B} = C_l - C_{l,D}$
3 - Calculation of the particulate TMs concentrations	
• $C_{SS,E} = K_{d\delta} \cdot C_d$ • $C_{SS} = \frac{C_{SS,E}\cdot[SS]_R+C_{soil}\cdot[SS]_{NR}}{[SS]}$	• $C_{SS,D} = \frac{K_{d\delta}\cdot C_{d,D}\cdot[SS]_R}{[SS]}$ • $C_{SS,B} = \frac{K_{d\delta}\cdot C_{d,G}\cdot[SS]_R+C_{soil}\cdot[SS]_{NR}}{[SS]}$
5 - Calculation of the K_d	
$K_d = \frac{C_{SS}}{C_l}$; $K_{d,D} = \frac{C_{SS,D}}{C_{l,D}}$; $K_{d,B} = \frac{C_{SS,B}}{C_{l,B}}$	

3 Material

The model was applied to determine the variability depending on the river discharge of the K_d of ^{137}Cs in the SS of the downstream part of the Rhône River (south of France). Its results were compared to time-series of liquid and particulate ^{137}Cs concentrations and their corresponding ratio measured between 2005 and 2018 at the IRSN monitoring station, SORA, which is located on the Rhône downstream of all the nuclear facilities (Figure 3).

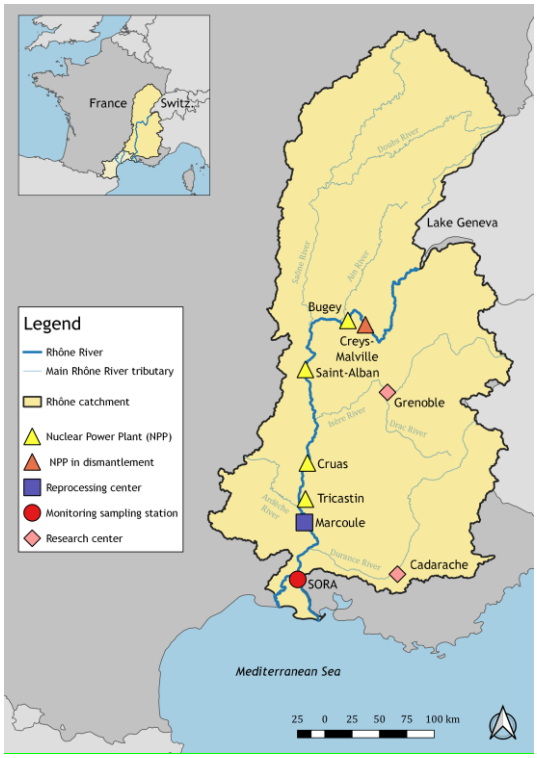

Figure 3: Rhône River and IRSN monitoring station SORA

The IRSN monitoring station SORA and its sampling protocol for SS and filtered water are detailed in Antonelli *et al*. (2008), Eyrolle *et al*. (2012) and Eyrolle *et al*. (2020). Outside flood periods, a composite sample resulting from samples taken every 80 minutes is collected over a period of about one month. During flood periods (> 3 000 $m^3.s^{-1}$), the composite sample is produced using samples taken every 60 minutes over 8 hours. Radionuclide analyses are performed on the particulate fraction (suspended sediments, SS) and on the dissolved fraction (fraction less than 0.5 µm, filtered waters, FW).

The representativeness of these data in terms of K_d depends on the validity or otherwise of the equilibrium of the solid / liquid fractionation of the ^{137}Cs contained in these samples according to its origin, its transit time in the river and the delay between the sampling and the filtration.
At the SORA station, the main sources of ^{137}Cs are the contamination of the soils of the watershed (cf. 3.4) and the discharges of the Marcoule Center (cf. 3.5). While the contamination of the watershed is old enough to assume a complete equilibrium and consequently a real K_d, the interpretation is less obvious for the discharges of the Marcoule Center which is located 65 km upstream from the SORA station for a transit time close to one day. During this transit time, it can be considered that the processes of solid/liquid fractionation is dominated by the sorption

processes, for which equilibrium conditions are reached after one or two hours (Pérez, 2015). Consequently, it can be assumed that the solid/liquid ratios of ^{137}Cs in the Rhône at the level of the SORA station are a combination between the sorption K_d (cf. 1) of the Marcoule discharges and the real K_d of the watershed. However, it must also be considered that these conditions are not exactly those measured by the SORA station in reason of the sampling procedure which increases the contact time over a period of one month allowing to reach a quasi-equilibrium for the solid/liquid ^{137}Cs concentrations in the samples. This is partially demonstrated by the good agreement between the solid/liquid ratio measured at the SORA station and the distribution of the desorption K_d compiled in the framework of the AMORAD program of the International Agency of Energy Atomic (IAEA) (Boyer *et al.*, 2018; Tomczak *et al.*, 2019).

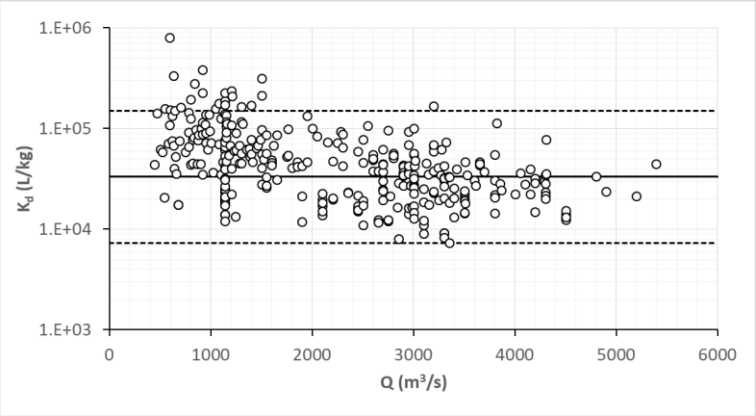

Figure 4: ^{137}Cs solid/liquid ratio measured at the SORA station *vs* IAEA distribution of SS desorption Kd.

(Dataset (points), IAEA conditional geometric mean (full line) and IAEA 5^{th} and 95^{th} percentiles (dotted lines)

Consequently, it can be assumed that the solid / liquid ratios determined from the data of the SORA station are probably representative of the K_d of ^{137}Cs in the Rhône at this station but not necessarily of the state of the solid / liquid fractionation which crosses the section of sampling.

In complement, the distance and the transfer time between the Marcoule Center and the SORA station permit also to assume as correct the assumption of complete mixing and the use of Equation 12 (cf. Section 2).

3.1 Calculation procedure

As the ^{137}Cs concentrations and the model input parameters (Table 1) were not all available at the same time, the variabilities of the solid and liquid concentrations and K_d were modeled by considering the conditional statistical distribution of [SS] and r according to the river discharge and the statistical distributions, over the period 2005-2018, of C_{soil} and C_D. The range of river discharges was scanned between Q_{MIN} (400 $m^3.s^{-1}$) and Q_{MAX} (6000 $m^3.s^{-1}$). For each water flow rate, several sets of input parameters were determined with a weighted Latin hypercube method which consisted of four imbricated loops scanning between their 2^{nd} and 98^{th} percentiles the conditional distributions of [SS] and r according to Q and the distributions of C_{soil} and $C_{D.}$ The result associated to each set of input parameters was weighted by the product of the probability densities of the different parameters. Finally, the geometric means and the minimal and maximal values of the modelled solid and liquid concentrations and K_d obtained at the different water flow rates were compared with the conditional statistical distributions of the dataset.

The calculation procedure was developed as an Excel macro written in Visual Basic Application language. For information, the calculation times on a laptop computer and with the parameters specified in Table 2 are approximately 15 seconds.

It was not possible to determine statistical distributions for the specific parameters of ^{137}Cs, δ and $K_{d\delta}$, because only the values published by Abril and Fraga (1996) were available:

$$\delta = 1.96\ \mu m \text{ and } K_{d\delta} = 68 \cdot 10^3\ l.kg^{-1}$$

Therefore, these two values were directly applied and used in the discussion. In the meantime, the statistical distributions of the other input parameters are detailed below.

3.2 Conditional statistical distribution of [SS] as a function of the river discharge

The conditional log-normal distribution of [SS] as a function of the river discharge was determined from data acquired between March 2001 and April 2008 at the SORA monitoring station (Eyrolle *et al.*, 2012). The conditional geometric means ($GM([SS]|Q)$), geometric standard deviations ($GSD([SS]|Q)$) and second and ninety-eighth percentiles ($2^{th}([SS]|Q)$ and $98^{th}([SS]|Q)$) were determined using a sliding window method (Tomszak et al., 2018) applied to this dataset classified according to the increasing water flow rates (Figure 5).

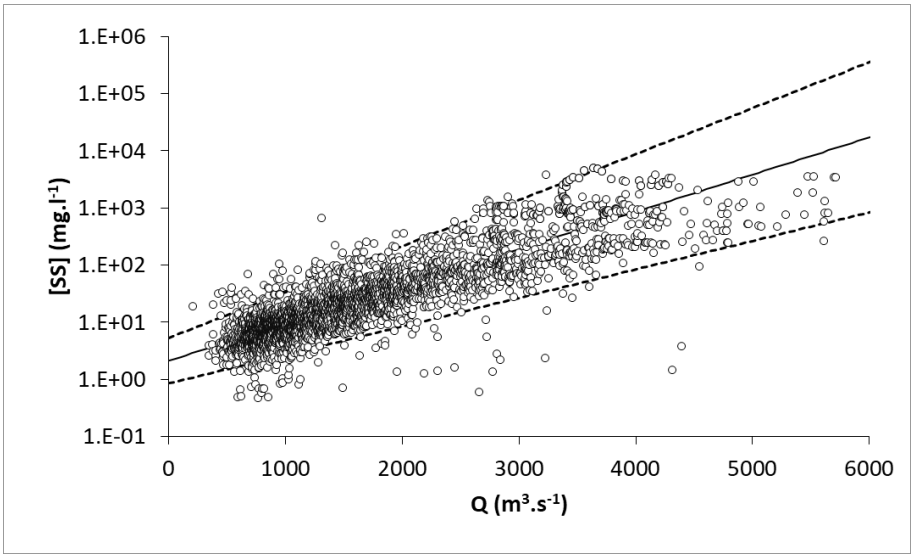

Figure 5: Suspended sediment concentrations versus Rhône River discharge at SORA station (Q, [SS]) dataset (points), conditional geometric mean (full line) and 2^{th} and 98^{th} percentiles (dotted lines)

The mean relationships obtained for $GM([SS]|Q)$ and $GSD([SS]|Q)$ are:

$$GM([SS]|Q) = 2.13 \cdot e^{0.0015 \cdot Q} \text{ [mg.l}^{-1}\text{] with } R^2 = 0.98 \quad \text{(Eq. 27)}$$

$$GSD([SS]|Q) = 1.56 \cdot e^{0.0002 \cdot Q} \text{ with } R^2 = 0.54 \quad \text{(Eq. 28)}$$

3.3 Conditional log-normal distribution of r as a function of the river discharge

The distributions of the radius r of SS as a function of the river discharge were determined from data of suspended sediments sizes distributions acquired with an hourly time step between December 2011 and August 2012 at the SORA station (Adell, 2013). In practice, one of the operational parameters to represent these distributions as a function of the water flow is r_{50}, i.e. the fiftieth percentile of the particle volume distribution. For the AFM, the consequences consecutive to the use of this parameter in place of the particle size distribution depend on the difference between $\left(1 - \frac{\delta}{r_{50}}\right)^3$ and $\sum_{r_i > \delta} f_i \cdot \left(1 - \frac{\delta}{r_i}\right)^3$ (see Eq. 8 and 9) where f_i is the frequency of the radius r_i.

Over the range of water flow rates covered by our particle size data, these two expressions differ by less than 20% at the same time that the variability of r_{50} is extended over a range greater than a factor 2 (ten times more) for each water flow condition (Figure 6). Therefore, and for this application case, using the variability of r_{50} instead of the particle size distributions enhances

the operational capabilities of the model without affecting the accuracy of the results. However, if this simplification is without consequences here, it is less suitable when applying the model to a specific suspension or in view to assess the transfers of TMs to deposited sediments for which the sedimentation / erosion processes increase the sorting of the particles according to their size and the hydraulic conditions

For water flow rates between 400 and 3000 $m^3.s^{-1}$, the data show that r_{50} vary between 3 and 10 µm (Figure 6) which is consistent with other results obtained on the Rhône River (Slomberg *et al.*, 2016) and rivers from the Humber and Tweed catchments (Walling *et al.*, 2000). For this range of water flow, the conditional log-normal distributions of r_{50} as a function of the river discharge were determined in the same way as for [SS]. Thus, the variability of r_{50} for water flow rates between 400 and 3000 $m^3.s^{-1}$ is covered by a conditional geometric mean ($GM(r_{50}|Q)$) represented by an equation of the second order (Eq. 29) and a constant conditional standard deviation ($GSD(r_{50}|Q)$) equal to 1.2 (Figure 6).

- If ($Q \leq 3000\ m^3.s^{-1}$) $\Rightarrow$

$$GM(r_{50}|Q) = 2.12 \cdot 10^{-6} \cdot Q^2 - 7.96 \cdot 10^{-3} \cdot Q + 13\ [\mu m]\ (R^2 = 0.65) \quad \text{(Eq. 29)}$$

$$GSD(r_{50}|Q) = 1.2 \quad \text{(Eq. 30)}$$

- If ($Q > 3000\ m^3.s^{-1}$) $\Rightarrow$

Beyond water flow rates of 3000 $m^3.s^{-1}$, the lack of data does not allow a detailed assessment of the variability of r_{50}. As a first approximation, this variability is extrapolated by considering Eq. 29 for $GM(r_{50}|Q)$ and by increasing $GSD(r_{50}|Q)$ from 1.2 for Q = 3000 $m^3.s^{-1}$ to 2 for Q = 6000 $m^3.s^{-1}$ (Figure 6):

$$GSD(r_{50}|Q) = (Q - 3000) \cdot \frac{2-1.2}{6000-3000} \quad \text{(Eq. 31)}$$

To assess the sensitivity of the model, the results obtained with this assumption are compared in the discussion (cf. Section 5) with those given by a reduced variability defined by a $GSD(r_{50}|Q)$ which decreases from 1.2 for Q = 3000 $m^3.s^{-1}$ to 1 for Q = 6000 $m^3.s^{-1}$.

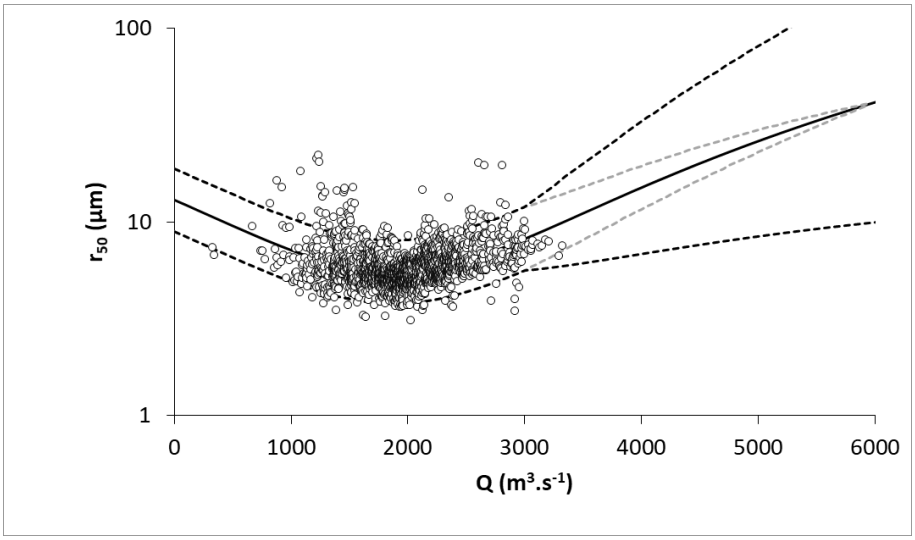

Figure 6: Mean radius r_{50} of suspended sediments vs Rhône River discharge at station SORA (Q, r_{50}) dataset (points) and conditional geometric mean (full line) and 2^{th} and 98^{th} percentiles (dotted lines) – Black for $GSD(r_{50}|6000) = 2$ and Grey for $GSD(r_{50}|6000) = 1$

3.4 Statistical distribution of the mean ^{137}Cs concentrations in the soils of the catchment

The background of the ^{137}Cs concentrations in the soils of the Rhône watershed is related to the atmospheric fallout from past nuclear tests and the Chernobyl accident (Perkins and Thomas, 1980; Duffa, 2001; Zebracki *et al.*, 2013a,b). This background was estimated between 11 and 19 Bq.kg^{-1} for the year 2003 (Antonelli *et al.*, 2008; Eyrolle *et al.*, 2012) and between 3 and 11 Bq.kg^{-1} for the year 2018 (Thollet *et al.*, 2018). Consequently, the variations of the minimal and maximal values of C_{soil} for the period 2003 to 2018 can be described by two exponential relations with an effective decay period of 7 years for the minimal values ($C_{soil,MIN}(y) = 11 \cdot e^{-0.1 \cdot (y-2003)}$) and of 16 years for the maximal values ($C_{soil,MAX}(y) = 19 \cdot e^{-0.042 \cdot (y-2003)}$) with y the considered year. These values are within the range of the values published in the scientific literature (Garcia-Sanchez, 2008). They are faster than the radioactive decay period of ^{137}Cs (30.2 years) because they aggregate the radioactive decay with several transfer processes such as wash-off, erosion, infiltration, etc...

The statistical distribution of C_{soil} between 2015 and 2018 was determined by discretizing these two curves with a yearly time step. For each year, the interval between the minimal and maximal values was discretized into 20 intervals with the assumption of uniform distribution. These steps provided a dataset of 260 soil activities which was statistically described by a log-normal distribution with $GM(C_{soil})$ = 9.8 Bq.kg^{-1} and $GSD(C_{soil})$ = 1.46 (R^2 = 0.99).

For each water flow rate, the distribution of C_{soil} was scanned between its 2th and 98th percentiles which were 4.5 and 21.3 Bq.kg^{-1}.

3.5 Statistical distribution of the industrial liquid discharges of ^{137}Cs

The main anthropogenic source of ^{137}Cs liquid discharges into the Rhône is the Marcoule spent nuclear fuel reprocessing plant which discharges one order of magnitude more than the other nuclear facilities along the Rhône River (Charmasson, 1998; Rolland, 2006). For the period 2005 to 2018, the fluxes of ^{137}Cs monthly discharged by the Marcoule center ranged from 10^2 to 10^4 MBq.month^{-1}. Considering the average monthly water flow rates and noting that the Marcoule center is not authorized to discharge when the water flow rate of the Rhône exceeds 4000 m^3.s^{-1} at its lower part (Zebracki *et al.*, 2015), these releases lead to added monthly activities ranging between $2{\cdot}10^{-4}$ and $2{\cdot}10^{-3}$ Bq.l^{-1} over the period 2005-2019 (Figure 7).

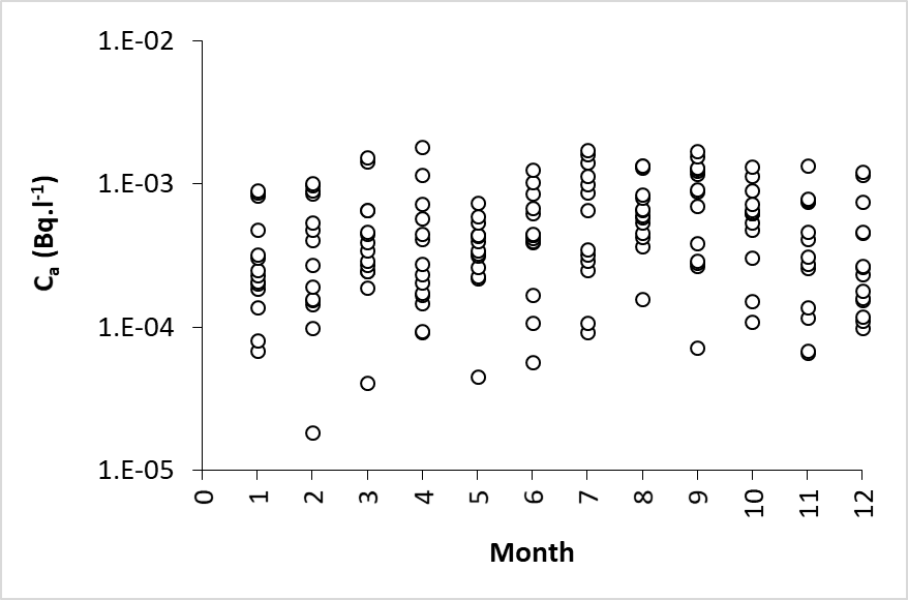

Figure 7 : Theoretical average monthly concentrations of ^{137}Cs added by the liquid discharges of the Marcoule Center

Figure 7 shows that the variability of the added concentrations from industries does not depend on the month that is suggested to consider the entire variability whatever the river discharge. This variability is represented by a log-normal law defined by GM(C_D) = $3.9{\cdot}10^{-4}$ Bq.l^{-1} and GSD(C_D) = 2.43 (R2 = 0.99).

For each water flow rate, the distribution of C_D was scanned between the 2th and the 98th percentiles which are $6.23 \cdot 10^{-5}$ and $2.40 \cdot 10^{-3}$ Bq.l^{-1}.

4 Results

Table 2: Summary of the input parameters

Parameter	Law	Range	N$^{(*)}$
δ	n.r	1.96 µm	n.r
$K_{d\delta}$	n.r	$68 \cdot 10^4$ l.kg^{-1}	n.r
Q	n.r	0 – 6000 m^3.s^{-1}	40
[SS]	**Conditional log-normal as a function of Q** $GM([SS]\|Q) = 2.13 \cdot e^{1.5 \cdot 10^{-3} \cdot Q}$ $GSD([SS]\|Q) = 1.56 \cdot e^{0.0002 \cdot Q}$	2th([SS]|Q) - 98th([SS]|Q)	10
f_c	Discussed in results section	See results section	n.r
r_{50}	**Conditional log-normal as a function of Q** $GM(r_{50}\|Q) = 2.12 \cdot 10^{-6} \cdot Q^2 - 7.96 \cdot 10^{-3} \cdot Q + 13$ If $(Q \leq 3000) \Rightarrow GSD(r_{50}\|Q) = 1.2$ If $(Q > 3000) \Rightarrow GSD(r_{50}\|Q) = (Q - 3000) \cdot \frac{0.8}{3000}$	2th(r_{50}|Q) - 98th(r_{50}|Q)	10
Csoil	**Log-normal** GM(C_{soil}) = 9.8 Bq.kg^{-1} GSD(C_{soil}) = 1.46	4.5 – 21.3 Bq.kg^{-1}	10
Ca	**Log-normal if Q < 4000 m^3.s^{-1}** GM(Ca) = $3.9 \cdot 10^{-4}$ Bq.l^{-1} GSD(Ca) = 2.43 if Q > 4000 m^3.s^{-1} then C_a = 0 Bq.l^{-1}	$6.2 \cdot 10^{-5}$ – $2.4 \cdot 10^{-3}$ Bq.l^{-1}	10

$^{(*)}$N is the number of intervals for scanning the statistical distributions between their 2th and 98th percentiles. For each distribution, N was determined incrementally until no significant change was observed.

n.r: non relevant

Table 2 summarizes the input parameters applied for the calculations and Figure 8 compares, as a function of the river discharge, the raw values (points) and sliding geometric means (black lines) of the particulate and dissolved concentrations and K_d of ^{137}Cs to their modelled conditional geometric means (red lines) and modelled conditional minimum and maximum values (dashed red lines).

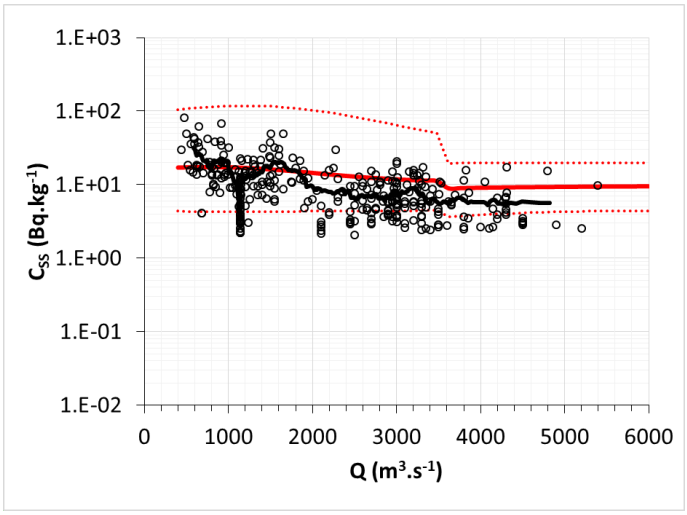

(a)

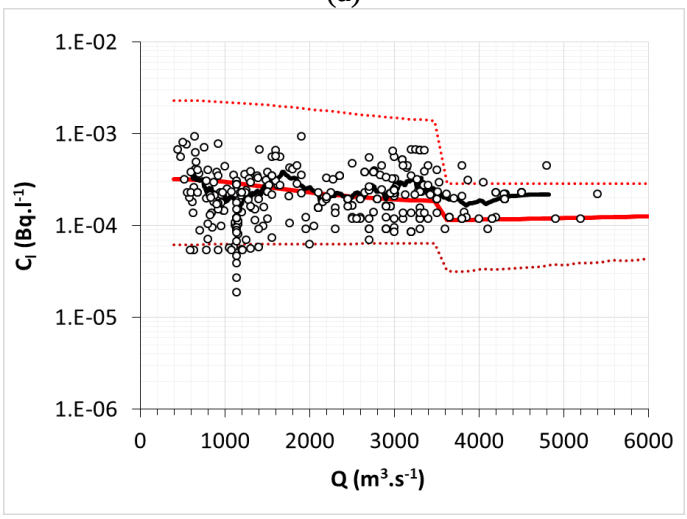

(b)

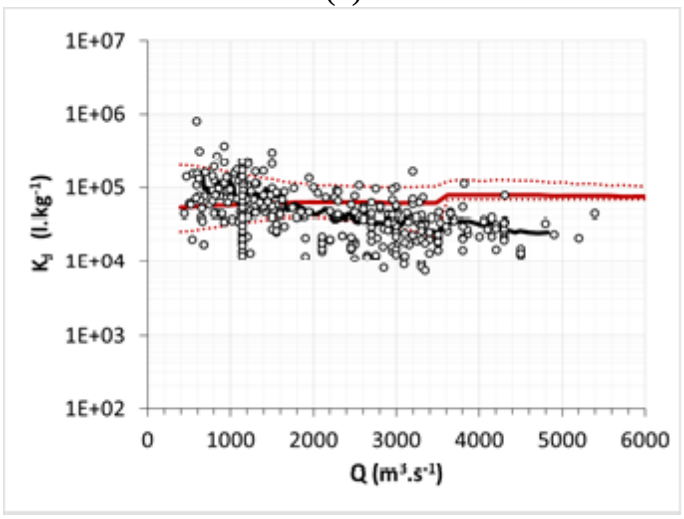

(c)

Figure 8: C_{SS}, C_l and K_d of ^{137}Cs: raw values (open circles) and sliding geometric means (black full lines) measured at the SORA station from 2005 to 2018 vs conditional geometric means (red full lines) and conditional minimum and maximum values (red dashed lines) modelled with the parameters of Table 2

Figure 8 (a) and (b) show that, without any calibration, the variabilities and the mean values given by the model for the particulate and liquid concentrations are very close to those measured: less than a factor of 2 on average. The modelled variability of K_d (Figure 8c) is in the same range as those measured when the water flow rates are less than 2000 $m^3.s^{-1}$. Beyond that, the model underestimates the variability and overestimates the mean values of K_d and the first idea that comes to mind to improve the modelling is to reduce $K_{d\delta}$ which seems closer to $20\text{-}30 \cdot 10^3$ $l.kg^{-1}$ than to $68 \cdot 10^3$ $l.kg^{-1}$. If this change effectively improves the modelling of K_d for water flow rates greater than 2000 $m^3.s^{-1}$, it induces also an underestimation of the particulate activities and K_d at lower water flow rates.

Therefore, reducing $K_{d\delta}$ is not the right way to improve the modelling of K_d over the entire range of water flow rates because this improvement requires increasing the dissolved activities without modifying the particulate ones. In practice, the only way to obtain this result is to introduce a colloidal pumping. Indeed, the modelling of the mean and the variability of K_d becomes correct over the entire range of water flows by applying $[SC] = \frac{f_c}{100} \cdot [SS]$ with $f_c \approx 3\%$ (Figure 9).

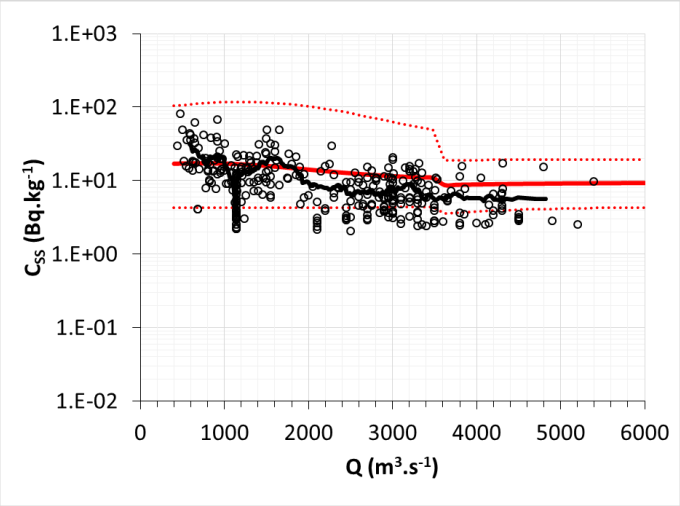

(a)

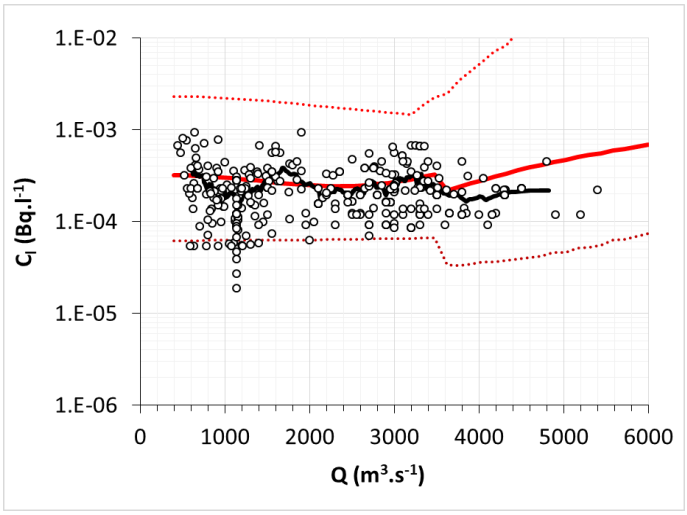

(b)

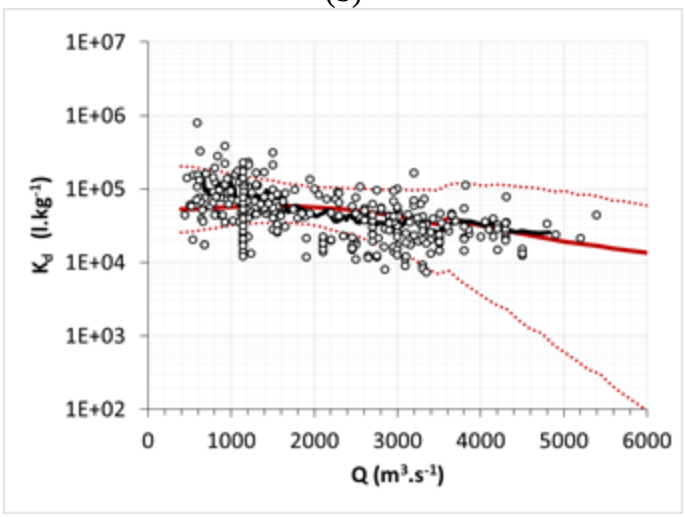

(c)

Figure 9 : C_{SS}, C_l and K_d of ^{137}Cs: raw values (open circles) and sliding geometric means (black full lines) measured at the SORA station from 2005 to 2018 vs conditional geometric means (red full lines) and conditional minimum and maximum values (red dashed lines) modelled with the parameters of Table 2 and $[SC] = 0.03 \cdot [SS]$

The small amount of data available on the Rhône colloids contents are consistent with $f_c \approx 3\%$ and support the hypothesis of a colloidal pumping effect. Slomberg *et al*. (2016) measured a colloidal content of 1% for a suspended load of 50 mg.l^{-1} and the modelled ^{137}Cs concentrations in colloids (C_c, Eq. 18) are in agreement with measurements performed at the SORA station by Eyrolle and Charmassson (2004) (Figure 10).

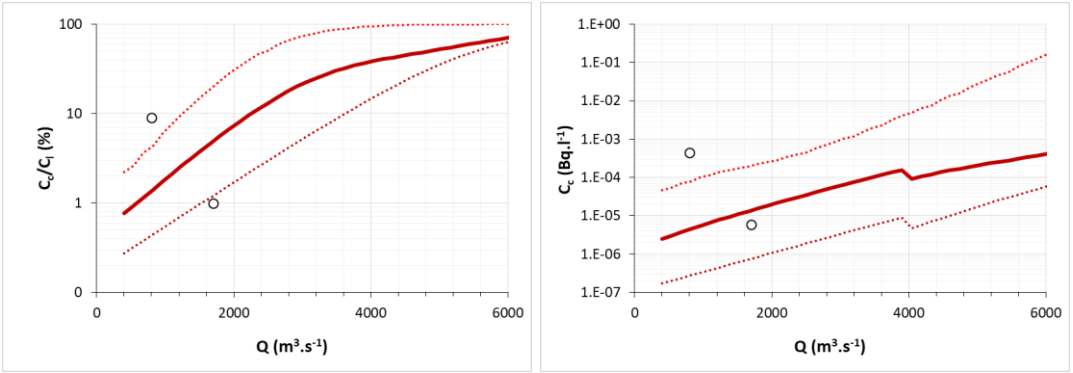

(a) (b)

Figure 10 : Cc/C_l and Cc: data measured at the SORA station by Eyrolle and Charmassson (2004) (open circles) vs conditional geometric means (red full lines) and conditional minimum and maximum values (dashed red lines) modelled with the parameters of Table 2 and $[SC] = 0.03 \cdot [SS]$

Figure 10 shows that the contribution of the colloidal fraction to the liquid ^{137}Cs concentration becomes significant (C_c/C_l mean > 10 %) when the river discharge exceeds 2000 $m^3.s^{-1}$ and suggests it can become dominant above 4000 $m^3.s^{-1}$. The threshold of 2000 $m^3.s^{-1}$ corresponds to a change in the hydro-sedimentary regime of the Rhône River which is illustrated by the dynamic of the r_{50} according to the water flow which increases faster above 2000 $m^3.s^{-1}$ (Figure 6). The aim of this paper is not to discuss the origin of this change, also observed on the dynamic of [SS] by Sadaoui *et al.* (2016), but it may correspond to a change in the erosion regime of the river with an erosion of the stocks of deposited sediments. In this case, two hypotheses could explain the colloidal pumping of ^{137}Cs in the Rhône River: 1) colloids mainly originate from the erosion of bottom sediments and/or river banks and they adsorb ^{137}Cs from industrial releases once they are in the water column, 2) colloidal forms of ^{137}Cs are directly produced by the erosion of ^{137}Cs sedimentary stocks accumulated since the previous erosive event. This last hypothesis is however not confirmed by the data and the model. Indeed, the remobilisation of colloidal forms of ^{137}Cs from sedimentary stocks would lead theoretically to an increase of the activities of ^{137}Cs within the filtered waters which is not supported by the measured concentrations which remain almost constant within their variability range, whatever the water flow rate (Figure 9b). Besides, this hypothesis would require introducing into the model a secondary source term which does not seem necessary here.

On another hand, the importance to consider the catchment background is well demonstrated by comparing the variabilities of the solid and liquid ^{137}Cs concentrations and of the K_d specifically to the background of the watershed and the industrial discharges (Eq. 26) respectively represented on Figure 11 by the blue and red lines.

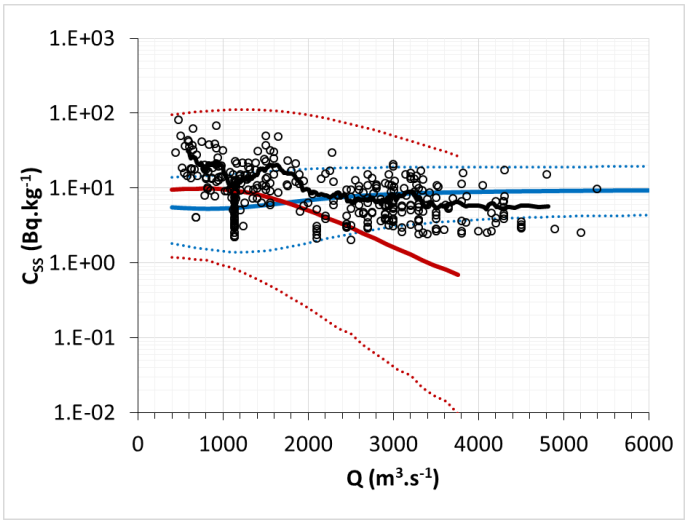

(a)

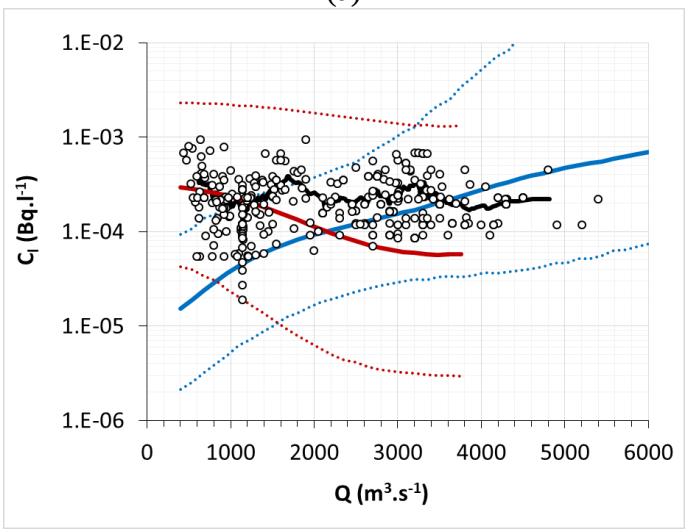

(b)

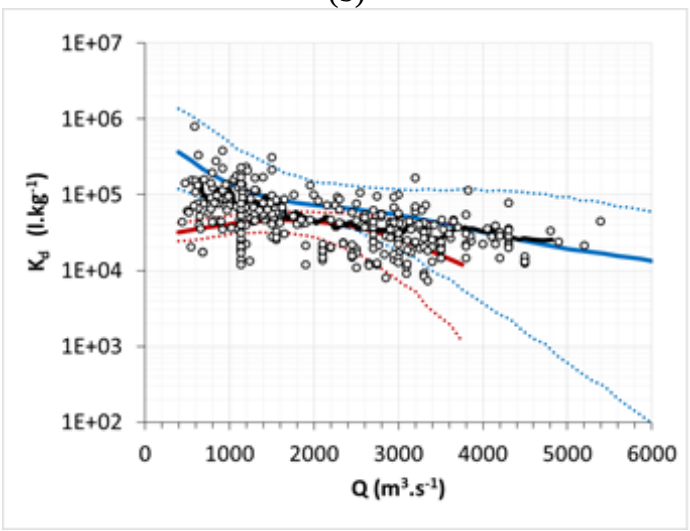

(c)

Figure 11 : C_{SS}, C_l and K_d of ^{137}Cs: raw values (open circles) and sliding geometric means (black full lines) measured at the SORA station from 2005 to 2018 vs conditional geometric means (full lines) and conditional minimum and maximum values (dashed lines) modelled with the parameters of Table 2 and $[SC] = 0.03 \cdot [SS]$ for the contributions of the background of the watershed (blue lines) and the industrial discharges (red lines)

For C_{SS}, (Figure 11a) the industrial discharges and background contributions are close below 2000 $m^3.s^{-1}$. Above this water flow rate, the background contribution becomes more and more dominant because of the increase in [SS] and r_{50}. Figure 11b shows that C_l is essentially linked to the anthropogenic discharges at low water flow rates and to the catchment background after 2000 $m^3.s^{-1}$. Figure 11c shows that the K_d of the anthropogenic releases is lower than the K_d of the geochemical background regardless of the river discharge. Above 4000 $m^3.s^{-1}$, where there are no anthropogenic discharges (see 3.4), the model reproduces correctly the mean K_d that translates the strong dependence of this variable to the catchment background.

5 Discussion

At this stage, one must remember that the model very faithfully reproduces the average trends and variabilities of C_{SS}, C_l and K_d of ^{137}Cs as a function of the water flow rate of the Rhône and without requiring an additional calibration than that of the colloidal fraction in the suspension. This result is all the most surprising since no variabilities were considered for the chemical parameters of ^{137}Cs, δ and $K_{d\delta}$, for which we directly considered the values obtained by Abril (1998b) from the laboratory experiments of He and Walling (1996) on soil and sediment particles totally independent from the Rhône.

To better appreciate the representativeness of these two parameters, Figure 12 presents the changes in K_d depending on whether $K_{d\delta} = 30{\cdot}10^3$, $68{\cdot}10^3$ and $140{\cdot}10^3$ $l.kg^{-1}$.

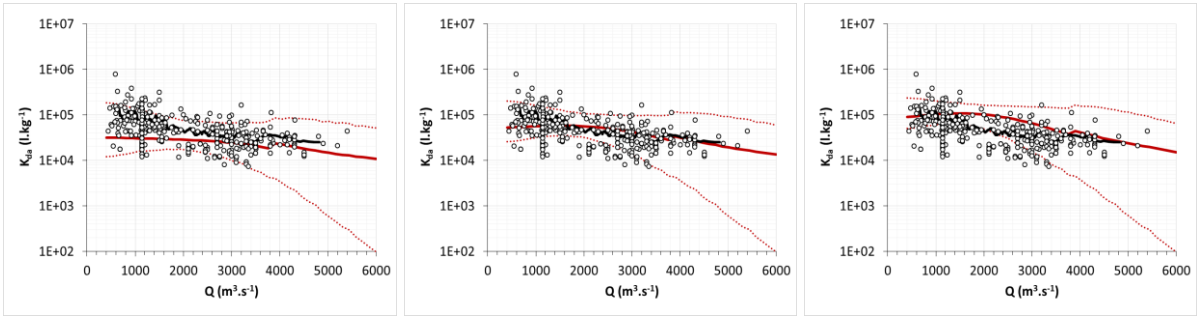

(a) (b) (c)

Figure 12 : Variabilities of K_d as a function of the river discharge for δ = 1.96 µm and $K_{d\delta}$ = $30{\cdot}10^3$ (a), $68{\cdot}10^3$ (b) and $140{\cdot}10^3$ (c) $l.kg^{-1}$.
(Open circles: data measured at the SORA station from 2005 to 2018; Black full line: sliding geometric mean of raw data; Red full line: modelled geometric means; Red dashed lines: modelled minimal and maximal values)

$K_{d\delta}$ moves the geometric means vertically without significantly affecting the amplitude of the variability. The best results are obtained with the $K_{d\delta}$ value of Abril (1998b) which highlights

its strong representativeness, especially since a change less than a factor of two is enough to reduce the accuracy of the modelled mean curve.

Figure 13 presents the changes in K_d depending on whether δ = 1, 1.96 and 4 µm.

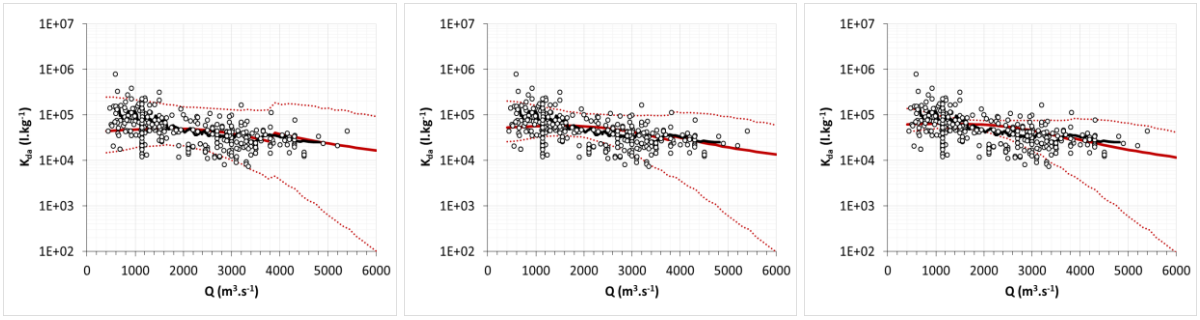

(a) (b) (c)

Figure 13: Variabilities of K_d as a function of the river discharge for δ = 1 (a), 1.96 (b) and 4 (c) µm and $K_{d\delta} = 68 \cdot 10^3$ l.kg^{-1}.
(Open circles: data measured at the SORA station from 2005 to 2018; Black full line: sliding geometric mean of raw data; Red full line: modelled geometric means; Red dashed lines: modelled minimal and maximal values)

Compared to $K_{d\delta}$, Figure 13 shows that the variations of δ affect the amplitude of the variability of K_d without significantly modifying the geometric means. The lower δ is, the greater is the variability of K_d because the contribution of the non-exchangeable fractions (representative of the geochemical background of the watershed) decreases at the same time as δ.

Comparison between the modelled variability and the dataset shows that δ cannot be greater than the value given by Abril (1998b) and suggests that the variability of the dataset is better represented by δ = 1 µm. Consequently, an uncertainty can be assumed for δ ($1 < \delta < 2$ µm) but it remains limited to a factor of 2, which once again confirms the strong representativeness of the value published by Abril (1998b).

For water flow rates greater than 3000 m^3.s^{-1} the main uncertainty is linked to the lack of data for r_{50} (cf. 3.5). If the right agreement between the modelled and measured geometric means allows to consider as acceptable the Equation 29 for the evolution of $GM(r_{50}|Q)$, it remains an uncertainty about the effect of the strong variability associated to r_{50} for this range of water flow rates (cf. 3.5). To assess this effect, Figure 14 compares the results obtained with this variability to those obtained with the reduced variability of r_{50} defined by a $GSD(r_{50}|Q)$ decreasing from 1.2 for Q = 3000 m^3.s^{-1} to 1 for Q = 6000 m^3.s^{-1} (Figure 6).

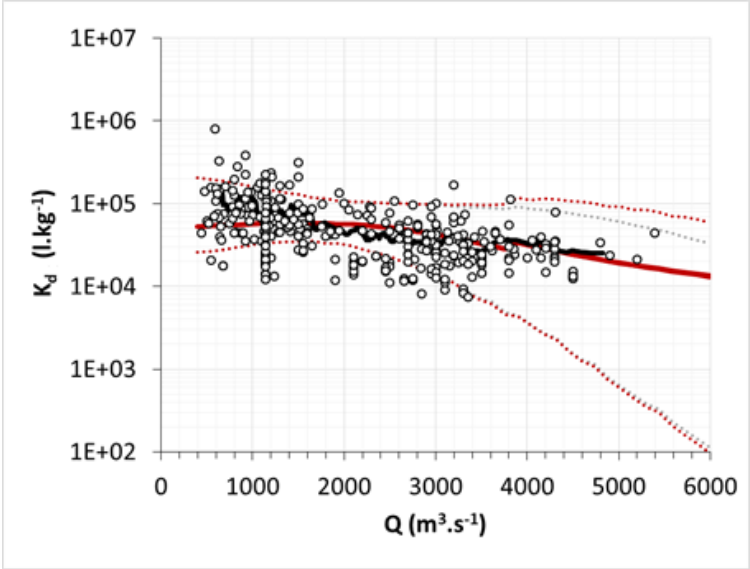

Figure 14 : K_d of ^{137}Cs modelled with a high variability of r_{50} (red lines) *vs* modelling with a low variability of r_{50} (grey lines)
(Open circles: data measured at the SORA station from 2005 to 2018; Black full line: sliding geometric mean of raw data; Red full line: modelled geometric means; Red and Grey dashed lines: modelled minimal and maximal values)

This figure shows few effects of the variability of r_{50} on the modelling of the K_d distributions for water flow rates larger than 3000 $m^3.s^{-1}$. Just appears a light decreasing of the maximal K_d values explained by the greater minimal particle sizes induced by the lower variability. However, the effects are limited and quasi-invisible for the minimal K_d values. For water flow rates larger than 3000 $m^3.s^{-1}$, this behaviour of the model is essentially explained by the colloidal loads which increases at the same time that the suspended load. When the water flow rate increases, the modelled K_d values are thus more and more controlled by the colloidal pumping and less and less by the particle size as it is shown by comparison of Figure 8c (without colloidal pumping) and Figure 9c (with colloidal pumping). From an operational point of view this result suggests that the attention payed to the colloidal phases of TMs is all the more important that the water flow rate is strong.

These results highlight both the correct behaviour of the model and its robustness. They motivate to extend its application to other TMs than ^{137}Cs and to rivers other than the Rhône, the input data being the average concentrations of TMs in the soils of the watershed, the anthropogenic discharges and the load and the average size of the SS as well as the colloidal load as a function of the water flow. Under the present form of the model, the main constraints are the checking of the mixing conditions and the transit time since the anthropogenic discharges and, probably the most important, the knowledge for each TM of δ, the thickness of the exchange layer and $K_{d\delta}$, its specific K_d. The results obtained here suggest that these two parameters could have a generic representativeness if they are determined independently of the

hydro-sedimentary conditions, which would be possible from laboratory experiments, by adjustment with *in-situ* data and/or with geochemical models.

From a general point of view, this work demonstrated that the variability of the K_d of SS in rivers does not only depend on the chemical conditions but also and rather on the hydro-sedimentary conditions as previously shown by Cho et al. (2016), the discharges and the context of the watershed. These considerations suggest that this modelling approach could contribute to the prediction of the impact of changes in erosion regimes of rivers and watersheds on the TMs transfers in rivers, for example in a context of climate change. In this case, the model will have to be coupled with hydro-sedimentary models capable of predicting the impact of these changes on the hydro-sedimentary properties of the river.

6 Conclusions

This paper reports an adaptation of the model of Abril and Fraga (1996) to model the K_d of trace metals in suspended sediments of rivers as a function of the river discharge, the load and the mean particle size of suspended sediments, the colloidal pumping effect, the geochemical and anthropogenic backgrounds of the watershed and the industrial discharges. The application to the case of ^{137}Cs in the Rhône River highlights the fact that the variability of the ^{137}Cs K_d is essentially explained by the geochemical and anthropogenic backgrounds of the catchment, the industrial discharges and the changes, as a function of the river discharge, of the load and mean size of suspended sediments. This illustrates how much the variability of K_d of suspended sediments is not dependent only on chemical processes and must be considered from a larger point of view, that include the hydro-sedimentary processes and the catchment context. This is not very surprising considering that the non-exchangeable fractions of trace metals are poorly reactive to changes in chemical conditions and that, at the temporal and spatial scales of a river, the impact of these changes remains limited compared to the hydro-sedimentary forcing. These results highlight also the strong representativeness of the specific chemical parameters such as the parameters δ and $K_{d\delta}$ of the Abril and Fraga Model and lead us to suggest focalizing the geochemical models of K_d on the determination of this kind of parameters or equivalent ones.

Acknowledgements

The present work was carried out within the framework of the GGP collaboration program between EDF and IRSN and the authors thank these institutions for their support and funding.

References

Abarca M., Guerra P., Arce G., Montecinos M., Escauriaza C., Coquery M., Pastén P. (2017). Response of suspended sediment particle size distributions to changes in water chemistry at an Andean mountain stream confluence receiving arsenic rich acid drainage. Hydrological Processes, 31, pp. 296-307.

Abril J.M., Fraga E. (1996). Some physical and chemical features of the variability of K_d distribution coefficients for radionuclides. J. Environ. Radioactivity 30(3), pp. 253-270.

Abril J.M. (1998)a. Basic Microscopic Theory of the Distribution, Transfer and Uptake Kinetics of Dissolved Radionuclides by Suspended Particulate Matter - Part I: Theory Development. J. Environ. Radioactivity, 41(3), pp. 307-324.

Abril J.M. (1998)b. Basic Microscopic Theory of the Distribution, Transfer and Uptake Kinetics of Dissolved Radionuclides by Suspended Particulate Matter — Part II: Applications. J. Environ. Radioactivity, 41(3), pp. 325-342.

Adell W. (2013). Caractérisation de la distribution granulométrique des particules en transit dans le Rhône aval au cours du temps et des conditions hydrologiques. Rapport stage Master Sciences de l'Eau et de l'Environnement - Hydrosystèmes et Bassins Versants : diagnostic et risque environnemental. 51 pp.

Allison J.D., Allison T.L. (2005). Partition coefficient for metals in surface water, soil, and waste. EPA/600/R-05/074 Washington, DC, United States.

Antonelli C., Eyrolle F., Rolland B., Provansal M., Sabatier F. (2008). Suspended sediment and ^{137}Cs fluxes during the exceptional December 2003 flood in the Rhône River, southeast France. Geomorphology, 95, pp. 350-360.

Apte S.C., Benko W.I., Day G.M. (1995). Partitioning and complexation of copper in the Fly River, Papua New Guinea. Journal of Geochemical Exploration 52(1-2), pp. 67-79.

Barreto S.R.G., Barreto W.J., Deduch E.M. (2011). Determination of partition coefficients of metals in natural tropical water. Clean Soil, Air, Water, 39(4), pp. 362-367.

Benoit G., Rozan T.F. (1999). The influence of size distribution on the particle concentration effect and trace metal partitioning in rivers. Geochimica et Cosmochimica Acta, 63(1), pp. 113-127.

Boszke L., Kowalski A., Siepak J. (2004). Grain size partitioning of mercury in sediments of the middle Odra River (Germany/Poland). Water Air and Soil Pollution, 159, pp. 125-138.

Boyer P., Wells C., Howard B. (2018). Extended K_d distributions for freshwater environment. J. Environ. Radioactivity, 192, pp. 128-142.

Cameron, D. A., Klute, A. (1977). Convective-dispersive transport with a combined kinetic and equilibrium model, Water Resour. Res., 13**,** pp. 183-188.

723 Charmasson, S. (1998). Cycle du combustible nucléaire et milieu marin – Devenir des effluents
724 rhodaniens en Méditerranée et des déchets immergés en Atlantique nord-est. Thèse de
725 doctorat d'état, Université Aix-Marseille II, 365 pp.
726
727 Cho E., Arhonditsis G.B., Khim J., Chung S., Heo T.Y. (2016). Modelling metal-sediment
728 interaction processes: Parameter sensitivity assessment and uncertainty analysis.
729 Environmental Modelling & Software, 80, pp. 159-174.
730
731 Ciffroy P., Siclet F., Humbert B. (1995). In situ determination of 110m-Ag, 58-Co, 60-Co and
732 54-Mn distribution between freshwater and suspended matter. International Symposium on
733 Environmental Impact of Radioactive Releases, IAEA-SM-339/90, pp. 299-309.
734
735 Ciffroy P., Durrieu G., Garnier J-M. (2009). Probabilistic distribution coefficients (Kds) in
736 freshwater for radioisotopes of Ag, Am, Ba, Be, Ce, Co, Cs, I, Mn, Pu Ra, Ru, Sb, Sr and
737 Th. – Implications for uncertainty analysis of models simulating the transport of
738 radionuclides in rivers, J. Environ. Radioactivity, 100(9), pp. 785-794.
739
740 Crosby B., Whipple K. (2004). Surface Processes and Landscape Evolution. Massachusetts
741 Institute of Technology: MIT OpenCourseWare.

742 Dominik J., Vignati D.A.L., Pereira de Abreu M.-H., Kottelat R., Szalinska E., Bas B.,
743 Bobrowski A. (2007). Speciation and environmental fate of chromium in rivers
744 contaminated with tannery effluents. Engineering in Life Sciences, 7(2), pp. 155-169.
745
746 Duffa C. (2001). Répartition du plutonium et de l'américium dans l'environnement terrestre de
747 la basse vallée du Rhône. Thèse de doctorat, Université Aix-Marseille III, 179 pp.
748
749 Duc T.A., Loi V.D., Thao T.T. (2013). Partition of heavy metals in a tropical river system
750 impacted by municipal waste. Environmental Monitoring and Assessment, 185, pp. 1907-
751 1925.
752
753 Durrieu G., Ciffroy P., Garnier J.M. (2006). A weighted bootstrap method for the determination
754 of probability density functions of freshwater distribution coefficients (Kds) of Co, Cs, Sr
755 and I radioisotopes. Chemosphere, 65(8), pp. 1308-1320.
756
757 Eyrolle F., Charmasson S. (2004). Importance of colloids in the transport within the dissolved
758 phase (<450 nm) of artificial radionuclides from the Rho ˆne river towards the Gulf of Lions
759 (Mediterranean Sea). J. Environ. Radioactivity, 72, pp. 273-286.
760
761 Eyrolle F., Duffa C., Antonelli C., Rolland B., Leprieur F. (2006). Radiological Consequences
762 of the extreme flooding on the lower course of the Rhône valley (December 2003, South
763 East France). Science of the Total Environment, 366, pp. 427-438.
764
765 Eyrolle F., Radakovitch O., Raimbault P., Charmasson S., Antonelli C., Ferrand E., Aubert D.,
766 Raccasi G., Jacquet S., Gurriaran R. (2012). Consequences of hydrological events on the
767 delivery of suspended sediment and associated radionuclides from the Rhône River to the
768 Mediterranean Sea. J Soils Sediments, 12, pp. 1479-1495.
769
770 Eyrolle F., Lepage H., Antonelli C., Morereau A., Cossonnet C., Boyer P., Gurriaran R. (2020).
771 Radionuclides in waters and suspended sediments in the Rhône River (France) - current

772 contents, anthropic pressures and trajectories. Science of the Total Environment, 723, pp.
773 137-873.
774
775 Fan J., Zhao G., Sun J. (2017). Binary component sorption of cadmium, and copper ions onto
776 Yangtze River sediments with different particle sizes. Sustainability, 9, 2089, 16 pp.
777
778 Garneau C., Sauvage S., Sanchez-Perez J.M., Lofts S., Brito D., Neves R., Probst A. (2017).
779 Modelling trace metal transfer in large rivers under dynamic hydrology: A coupled
780 hydrodynamic and chemical equilibrium model. Environmental Modelling & Software, 89,
781 pp. 77-96.
782
783 Garcia-Sanchez L. (2008). Watershed wash-off of atmospherically deposited radionuclides:
784 review of the fluxes and their evolution with time. J. Environ. Radioactivity, 99, pp. 563-
785 573.
786
787 Garcia-Sanchez L., Loffredo N., Mounier S., Martin-Garin A., Coppin F. (2014). Kinetics of
788 selenate sorption in soil as influenced by biotic and abiotic conditions: a stirred flow-through
789 reactor study. J. Environ. Radioactivity, 138, pp. 38-49.
790
791 Gibbs R.J., Matthews M.D., Link D.A. (1971). The relationship between sphere size and
792 settling velocity. Journal of Sedimentary Petrolology, 41, pp. 7-18.
793
794 Goldberg S., Criscenti L.J., Turner D.R., Davis J.A., Cantrell K.J. (2007). Adsorption –
795 desorption processes in subsurface reactive transport Modelling. Vadose Zone J., 6, pp. 407-
796 435.
797
798 He Q., Walling D.E. (1996). Interpreting particle size effects in the adsorption of ^{137}Cs and
799 unsupported ^{210}Pb by mineral soils and sediments. J. Environ. Radioactivity, 30(2), pp. 117-
800 137.
801
802 Heling R., Raskob W., Popov A., Zheleznyak M. (1999). Overview of hydrological dispersion
803 module - HDM of RODOS. RODOS Report Decision Support for Nuclear Emergencies.
804 RODOS-WG4-TN(99)18.
805
806 Honeyman B.D., Santschi P.H. (1988). Metals in aquatic systems - Predicting their scavenging
807 residence times from laboratory data remains a challenge. Environ. Sci. Technol., 22(8), pp.
808 862-871.
809
810 Ilina S.M., Marang L., Lourino-Cabana B., Eyrolle F., Boyer P., Coppin F., Sivry Y., Gélabert
811 A., Benedetti M.F. (2020). Solid/liquid ratios of trace elements and radionuclides during a
812 Nuclear Power Plant liquid discharge in the Seine River: Field measurements vs
813 geochemical modelling. J. Environ. Radioactivity, 220-221, 10 pp.
814
815 Jweda J., Baskaran M., van Heed E., Schweitzer L. (2008). Short-lived radionuclides (^{7}Be and
816 ^{210}Pb) as tracers of particle dynamics in a river system in southeast Michigan. Limnology
817 and Oceanography, 53(5), pp. 1934-1944.
818
819 Li Y.H., Burkhardt L., Buchholtz M., O'Hara P., Santschi P.H. (1984). Partition of radiotracers
820 between suspended particles and seawater. Geochimica and Cosmochimica Acta, 48, pp.
821 2011-2019.

Lu Y., Allen H.E. (2001). Partitioning of copper onto suspended particulate matter in river waters. Science of the Total Environment, 277, pp. 119-132.

Müller G., Förstner U. (1968). General Relationship between Suspended Sediment Concentration and Water Discharge in the Alpenrhein and some other Rivers. Nature, 217, pp. 244-245.

Palmateer G.A., McLean D.E., Kutas W.L., Meissner S.M. (1993). Investigations of suspended particulate-bacterial interaction in agricultural drains. Particulate matter and aquatic contaminants. Boca Raton; CRC Press.

Payne T.E., Brendler V., Comarmond M.J., Nebelung C. (2011). Assessment of surface area normalisation for interpreting distribution coefficients (K_d) for uranium sorption. J. Environ. Radioactivity, 102, pp. 888-895.

Peitzsch M., Kremer D., Kersten M. (2010). Microfungal alkylation and volatilization of selenium adsorbed by goethite. Environmental Science & Technology 44(1), pp. 129-135.

Pérez, F.F., Sweeck, L., Bauwens, W., Van Hees, M., Elskens, M. (2015). Adsorption and desorption kinetics of 60Co and 137Cs in fresh water rivers. J. Environ. Radioactivity, 149, pp. 81-89.

Perkins R.W., Thomas C.W. (1980). Worldwide fallout. Pages 53-82 in W.C. Hanson editor, ‘‘Transuranic elements in the environment’’, U.S. DOE, USA.

Reynolds R.A., Stramski D., Wright V.M., Woźniak S.B. (2010). Measurements and characterization of particle size distributions in coastal waters. Journal of Geophysical Research, 115(8), 19 pp.

Rolland B. (2006). Transfert des radionucléides artificiels par voie fluviale: conséquences sur les stocks sédimentaires rhodaniens et les exports vers la Méditerranée. Thèse de l’Université Paul Cézanne d’Aix-Marseille, 243 pp.

Sadaoui M., Ludwig W., Bourrin F., Raimbault P. (2016). Controls, budgets and variability of riverine sediment fluxes to the Gulf of Lions (NW Mediterranean Sea). J. Hydrol., 540, pp. 1002-1015.

Sigg L., Xue H., Kistler D., Schönenberger R. (2000). Size fractionation (dissolved, colloidal and particulate) of trace metals in the Thur River, Switzerland. Aquatic Geochemistry, 6, pp. 413-434.

Sheppard S.C., Long J., Sanipelli B., Sohlenius G. (2009). Solid/liquid partition coefficients (Kd) for selected soils and sediments at Forsmark and Laxemar-Simpevarp I. R-09-27, S R (Eds.), Swedish Nuclear Fuel and Waste Management Co, pp. 1402-3091.

Sheppard S.C., Sohlenius G., Omberg L.G., Borgiel M., Grolander S.N. (2011). Solid/liquid partition coefficients (Kd) and plant/soil concentration ratios (CR) for selected soils, tills and sediments at Forsmark. Svensk Kärnbränslehantering AB, SKB R-11-24. Stockholm, Sweden. Report. 77 pp. ISSN 1402-3091.

Slomberg D.,L., Ollivier P., Radakovitch O., Baran N., Sani-Kast N., Miche H., Borschneck D., Grauby O., Bruchet A., Scheringer M., Labille J. (2016). Characterization of suspended particulate matter in the Rhône River: insights into analogue selection. Environmental Chemistry, 13(5), pp. 804-815.

Thollet F., Le Bescond C., Lagouy M., Gruat A., Grisot G., Le Coz J., Coquery M., Lepage H., Gairoard S., Gattacceca J., Ambrosi J.-P., Radakovitch O. (2018). Observatoire des Sédiments du Rhône. Irstea.

Tipping E. (1994). WHAMC- a chemical equilibrium model and computer code for waters, sediments, and soils incorporating a discrete site/electrostatic model of ion-binding by humic substances. Journal of Compute Geoscience, 20, pp. 973-1023.

Tomczak W., Boyer P., Krimissa M., Radakovitch O. (2019). K_d distributions in freshwater systems as a function of material type, mass-volume ratio, dissolved organic carbon and pH. Applied Geochemistry, 105, pp. 68-77.

Town R.M., Filella M. (2002). Size fractionation of trace metal species in freshwaters: implications for understanding their behaviour and fate. Re/Views in Environmental Science & Bio/Technology, 1(4), pp. 277-297.

Turner A., Millward G.E. (2002). Suspended particles: Their role in estuarine biogeochemical cycles. Estuarine. Coastal and Shelf Science, 55, pp. 857-883.

Vuković Ž., Marković L., Radenković M., Vuković D., Stanković S. (2011). Heavy metal and bacterial pollution of the Sava River in Serbia. Archives of Industrial Hygiene and Toxicology, 62, pp. 11-16.

Walling D.E., Moorehead P.W. (1989). The particle size characteristics of fluvial suspended sediment : an overview. Hydrobiologia, 176/177, pp. 125-149.

Walling D.E., Owens P.N., Waterfall B.D., Leeks G.L.G., Wass P.D. (2000). The particle size characteristics of fluvial suspended sediment in the Humber and Tweed catchments, UK. Science of the Total Environment, 251/252, pp. 205-222.

Wang J., Baskaran M., Niedermiller J. (2017). Mobility of ^{137}Cs in freshwater lakes: A mass balance and diffusion study of Lake St. Clair, Southeast Michigan, USA. Geochimica et Cosmochimica Acta 218, pp. 323-342.

Warren L.A., Zimmerman A.P. (1994). The influence of temperature and NaCl on cadmium, copper and zinc partitioning among suspended particulate and dissolved phases in an urban river. Water Research, 28(9), pp. 1921-1931.

Xia X.M., Li Y., Yang H., Wu C.Y., Sing T.H., Pong H.K. (2004). Observations on the size and settling velocitydistributions of suspended sediment in the Pearl River Estuary, China. Continental Shelf Research, 24, pp. 1809-1826.

Zebracki M., Eyrolle F., Cagnat X., Antonelli C., De Vismes-Ott A., Boullier V. (2013)a. Characterization of naturally occurring radionuclides in the lower part of the Rhône River

waters (France), preliminary results from suspended sediments monitoring, Water Resources Management VII. WIT Trans. Ecol. Environ., 171, pp. 235-245.

Zebracki M., Eyrolle-Boyer F., De Vismes-Ott A., Antonelli C., Cagna X., Boullier V. (2013)b. Radionuclide contents in suspended sediments in relation to the flood types in the lower part of the Rhône River. Procedia Earth and Planetary Science, 7, pp. 936-939.

Zebracki M., Eyrolle-Boyer F., Evrard O., Claval D., Mourier B., Gairoarde S., Cagnat X., Antonelli C. (2015). Tracing the origin of suspended sediment in a large Mediterranean river by combining continuous river monitoring and measurement of artificial and natural radionuclides. Science of the Total Environment, 502, pp. 122-132.

Zhang Y., Zhang Y., Yu T. (2013). Quantitative characterization of Cu binding potential of dissolved organic matter (DOM) in sediment from Taihu Lake using multiple techniques. Frontiers of Environmental Science & Engineering, 8(5), pp. 666-674.